Synthesis and Characterization of Magneto-Plasmonic Hybrid Nanoparticles for Biomedical Applications

Sara Félix Medeiros dos Santos[1,2,3,*]

Supervisors: Prof. Dr. Marta Estrader Bofarull[2], Prof. Dr. Maria Clara Henriques Baptista Gonçalves[1]

Co-Supervisor: Prof. Dr. Xavier Batlle Gelabert[3]

[1] Instituto Superior Técnico, University of Lisbon, Lisbon, Portugal;

[2] Organic and Inorganic Chemistry Department, University of Barcelona, Barcelona, Spain;

[3] Condensed Matter Physics Department, University of Barcelona, Barcelona, Spain;

[*] sara.felix@tecnico.ulisboa.pt

October, 2021

Abstract

Cancer is one of the biggest causes of death in the world thus it is becoming increasingly important to improve cancer treatments and its early diagnosis. In this sense, a lot of research has been made in nanotechnology over the last few decades towards the implementation of new strategies to fight this disease. In this work, it was intended to synthesize spherical hybrid magneto-plasmonic nanoparticles, incorporating gold (Au) on the core and both gold and iron (AuFe) on the shell, that could further be translated into nanorods with the same composition, which would take advantages of both optical and magnetic properties of Au and Fe, respectively, along with its NIR(Near Infrared)-responsive feature provided by the rod shape.

Hence, the nanoparticles obtained would be capable of taking tasks such as improve magnetically-based imaging techniques by enhancing image contrast, improve magnetic hyperthermia treatments and optimize magnetically-guided drug delivery systems in a non-invasive way provided by its NIR-responsive nature thus providing targeted treatments and reducing the side-effects of the techniques currently used.

This way, the synthesis of gold nanoparticles was firstly performed aiming to use them as seeds to grow an AuFe shell afterwards. Throughout all the process, the protocols used were optimized and the nanoparticles were characterized on every step of the way.

Finally, the main goal of this work seems not to have been achieved, however it was possible to synthesize colloidally stable nanoparticles with a mean size of 3,3 nm containing 20% of iron and 80% of gold.

Keywords: Hybrid Magneto-Plasmonic Nanoparticles; Core-Shell; NIR-responsive; Nanorods

1. Introduction

Through the combination of more than one inorganic compound in the same nanomaterial it is possible to obtain nanohybrids with potential multifunctional properties since the coupling of multiple inorganic nanomaterials lead to a resulting nanohybrid with better therapeutic efficacy than their individual counterparts: if an individual inorganic compound is not suitable for a specific function into the desired application, it can be combined with a distinct inorganic compound which can improve a novel property to the resulting hybrid nanomaterial.

1.1. Hybrid Magneto-Plasmonic Nanoparticles

Particularly, hybrid magneto-plasmonic nanoparticles provide great interest into the biomedical field, considering that on one hand, magnetic NPs present the capacity of reacting to an external magnetic field, hence by manipulating this magnetic field it is possible to enhance the nanoparticles targeting efficiencies for drug delivery and imaging applications. On the other hand, plasmonic nanomaterials (namely, gold nanorods) present two major advantages on biomedical applications, being perhaps the most relevant one the fact that it exhibits strong absorption of an incident light, which is stronger when localized surface plasmon resonance (LSPR) occurs under the electromagnetic field with the resonance frequency. The other great interest of gold nanorods is the fact that the longitudinal plasmon resonance of rod-shaped nanomaterials can provide the absorption of wavelength radiation in the near-infrared (NIR) region,[1] also called the biological window. The NIR region enables deep penetration into biological tissues,[2] providing a great innovative feature to be implemented on medical applications, since the rate of absorption of this type of radiation by the living tissue is relatively low.[1]

Additionally, the tunability of the LSPR into the NIR region can overcome limited penetration of optical imaging systems and achieve efficient penetration into deep tissues. Therefore, to implement hybrid nanopar-

ticles with these properties combined would be a great achievement for its usage in biomedical applications.

In fact, nanoparticles possessing both magnetic and plasmonic properties in a single nano-object are highly promising for image-guided therapy, being able to provide more efficient treatments by incorporating imaging properties into therapeutics (i.e. theranostic applications).[3]

Since the improved properties of these hybrid NPs for biomedical applications are highly dependent on their shape, it can be changed in order to be NIR responsive,[4] which is a crucial and innovative feature concerning biomedical applications. Among all the possible shapes and conformations that these NPs can acquire, Janus NPs (i.e. NPs whose surfaces have two or more distinct physical properties) have attracted increased scientific interest in the technological and biomedical fields.

Furthermore, strong magnetic and NIR responsive plasmonic properties of engineered nanostars can overcome cellular and physiological barriers, target the entities of tumor environment, and induce physical therapeutic effects after being stimulated by a remote signal, thereby enabling a targeting treatment, which prevents the damage of surrounding healthy cells and limit the unwanted side effects of the treatments currently performed.[5] This represents an innovative research field on the implementation of novel drug delivery systems, since NIR-triggered controlled release of a therapeutic drug can provide the possibility of releasing the drug at the right location with the desired time and drug release rate,[3] while providing its protection and increasing its bioavailability.

Along with drug delivery applications, hybrid magneto-plasmonic NPs can bring a number of innovations on imaging applications. The combined magnetic and NIR-responsive plasmonic properties of these type of nanoparticles enable multimodal quantitative imaging combining advantageous functions of MRI, MPI, PAI and image guided drug delivery with controllable drug release,[3] thus it can overcome the disadvantages of each individual imaging technique by combining advantageous features from other imaging techniques. For instance, it has been proved that core-shell nanostars with SPIONs core and a gold star-shaped plasmonic shell were bounded to drug molecules and released upon NIR illumination due to the heat generation from the nanostars.[3]

Furthermore, it was demonstrated that Janus magneto-plasmonic nanoparticles, made of gold nanostars and iron oxide nanospheres are not only good nanoheaters for magnetic hyperthermia but also (and mostly) for photothermia.[5] Its NIR-responsive feature is advantageous for both optical imaging systems and laser-assisted biomedical applications[6] due to the high penetration efficiency of NIR light into deep tissues[3] without its damaging in a non-invasive way.

1.2. Brief state-of-the-art of Au-Fe based Nanorods

The main purpose of this work is to obtain hybrid nanoparticles with both gold and metallic iron, which remains a great challenge, being one of the biggest problems the fact that it is still very difficult to combine them without the risk of iron oxidation. This way, there is not a lot of articles on bibliography regarding this matter, however a lot of research has been made in the last decades in relation to hybrid nanoparticles composed by gold and iron oxide, given the high stability and simplicity of synthesis of iron oxide NPs, and the excellent stability, biosafety and surface modification facility of AuNPs.[7] Most of these hybrid NPs are core-shell shaped, and it has been showed that the room-temperature synthesis of core–shell magnetite–gold NPs are especially attractive if the gold shell completely covers the magnetic core, consequently protecting it from oxidation, minimizing possible toxicity, and enabling its functionalization with ligands.[8]

A wide variety of synthesis methods have been investigated when researching different shapes of hybrid iron oxide and gold NPs. Actually, various morphologies of these hybrids have already been developed including spherical and non-spherical core-shell nanoparticles, nanoflowers, nanorods, etc.,[4] leading to new interesting joined magnetic and optical properties.[9]

Regarding iron-gold alloy NPs, there are just a few articles published concerning this matter, as the miscibility of these two elements is very low. The synthesis method most commonly used is laser ablation,[10] since it is a relatively simple method in which there is no need to use capping and stabilizing agents or reductants and it allows to stabilize metastable phases. However, when using this technique, the main challenge is to have control over the shape and size of the synthesized NPs. The control over its shape is crucial to determine the properties of the synthesized nanoparticles, hence it is urgent to find an alternative technique that enables this control.

Regarding this, the protocol used in this work was based on the protocol developed by Chiang et al.,[11] in which monodisperse hybrid iron and gold-based nanoparticles were obtained by the reduction of gold acetate with 1,2-hexadecanodiol and thermal decomposition of iron pentacarbonyl with oleic acid and oleylamine as stabilizers. This protocol was adapted to incorporate gold nanoparticles as seeds to grow the alliance between gold and iron, aiming, ultimately to adapt this template-based protocol and to obtain Au-AuFe core-shell nanorods.

Besides the protocol developed by Chiang et al.,[11] there is also coloidal synthesis published by Kwizera et al.,[7] in which AuNPs smaller than 10 nm can be absorbed on the surface of SPIONs via electrostatic interactions to serve as nucleation sites to grow a gold shell and consequently form uniform iron oxide-gold core–shell NPs.

Thus, the work herein described aims to provide a

newly innovative synthesis method to obtain spherical Au-AuFe core-shell nanoparticles, which can subsequently be adapted to the formation of Au-AuFe core-shell nanorods.

2. Materials and Methodology

In order to obtain the desired core-shell nanoparticles, firstly small-sized gold NPs were synthesized and secondly, they were tested to be used as seeds to grow a gold and metallic iron hybrid shell.

2.1. AuNPs Synthesis

The gold nanoseeds were synthesized by a thermal decomposition method adapted from the protocol used by C. Shen et al.,[12] in which the solvent 1-octadecene (30 mL, Aldrich, 90%) was added to a 100 mL three neck flask along with both the oleic acid (4,5 mL, Aldrich, 90%) and oleylamine (6,0 mL, Aldrich, 70%), representing the surfactant and reducing agent of the gold precursor, respectively, in the initial part of the protocol, with vigorous stirring and heating at 120°C for 20 minutes. In the final part of this synthesis, the gold (III) chloride trihydrate (120 mg, Alfa Aesar, $HAuCl_4 \bullet H_2O$, 99.99%) diluted with 7,5 mL of solvent was injected and the temperature was increased to 150°C for half an hour. An atmosphere of nitrogen was kept inside the flask throughout the entire synthesis.

Afterwards, the samples were washed with isopropanol*, centrifuged for 8 minutes at 6000 RPM and re-dispersed in hexane.

2.2. Au-AuFe Core-Shell NPs Synthesis

The protocol used to synthesize the Au-AuFe core-shell nanoparticles was adapted from Chiang et al.,[11] in which the AuNPs previously synthesized were used as seeds to grow a AuFe shell via the reduction of gold (III) acetate (Alfa Aesar, $Au(COOCH_3)_3$, 99.9%) by 1,2-hexadecanediol (Aldrich, $C_{16}H_{34}O_2$, 90%) and the thermal decomposition of iron pentacarbonyl (ACROS Organics, $Fe(CO)_5$, 99.5%), using oleic acid (Aldrich, 90%) and oleylamine (Aldrich, 70%) as surfactants.

The first part of the protocol involves keeping the mixture of AuNPs seeds (0,089 mmol), gold precursor and its reducing agent, the surfactants and the solvent (10 mL), on vacuum at 120°C for 30 to 40 minutes until the hexane contained on the AuNPs sample was totally evaporated.

Into the second part of the protocol, the iron precursor was injected under an atmosphere of nitrogen and the temperature was increased to 250°C for one hour.

The ratio of AuNPs:Au:Fe used in this protocol was changed from 1:1:1 to 1:2:2, in order to study the influence of this ratio of the final NPs obtained. Since the reducing agent of the gold precursor was 1,2-hexadecanediol, the quantities in mol used for both reagents were the same. As for the amount of surfactants added, it was the same as the mol of AuNPs.

Afterwards, the samples were washed with isopropanol, centrifuged for 8 minutes at 6000RPM and re-dispersed in toluene.

The protocol was implemented using two different solvents with different polarities, 1-octadecene (Aldrich, 90%) and dioctyl ether (Aldrich, 99%), in order to test their influence on the final NPs obtained.

*The isopropanol was added to the reaction mixture as soon as possible in order to stop the reaction faster and thus prevent ostwald ripening,[13] in which the smaller NPs in solution would dissolve and deposit on larger NPs in order to achieve thermodynamic stability, hence leading to polydispersity rather than monodispersity.

On every synthesis performed in this work, small amounts of sample at different reaction times were characterized in order to study the reaction progress. However, the changes observed were not relevant enough to be reported.

2.3. Characterization Techniques

TEM: The images of TEM were carried out both in a JEOL JEM-1010 80kV microscope and in a Tecnai Spirit 120kV microscope, with EMCN copper coated grids. **UV-Vis Spectroscopy**: Cary 100 UV-visible spectrophotometer with Hellma Analytics QS high precision cells. **HRTEM**: JEOL JEM-2100 200kV high resolution microscope, with 200 Mesh agar scientific holey carbon grids. **EDX**: Xplore TEM of Oxford Instruments, with an Aztec control software. **XPS**: photoelectron spectrometer (ESCA), from Physical Electronics, model PHI 5500, covering the entire periodic table of elements, with the exception of H and He, with a depth of analysis not exceeding 10 nm and with an analysis chamber in ultra-high vacuum (UHV) working in the range of 10^{-8} Torr to 10^{-9} Torr of pressure. **XRD**: XRD spectrum was obtained with a *PANalytical X'Pert PRO MPD alpha1* powder diffractometer in *Bragg-Brentano* $\vartheta/2\vartheta$ geometry of 240 millimetres of radius, with a work power of 45 kV.

The values used for the distance between crystalline plans and the 2-ϑ degrees of both gold[14] and magnetite[15] were the ones published on the indicated bibliography, for the crystalline plan analysis carried out on the HRTEM images obtained throughout all this work and the peak analysis performed on the XRD spectrum obtained, respectively.

3. Results and Discussion

The results of both synthesis protocols used will be discussed on the following section.

3.1. AuNPs: Synthesis and Characterization

When synthesizing the AuNPs seeds, the main concern was to obtain colloidally stable NPs, since the presence of aggregates would lead to the cover up of this same aggregates on the second step of this work rather than the formation a shell around each individual particle,

as intended. Secondly, it was also important to synthesize monodisperse NPs with relatively low size, since they are meant to be implemented on biomedical applications, and for this purpose small-sized NPs are preferred, since its diameter should be more than enough to circulate though out the blood circulatory network for sustained period of time.[16]

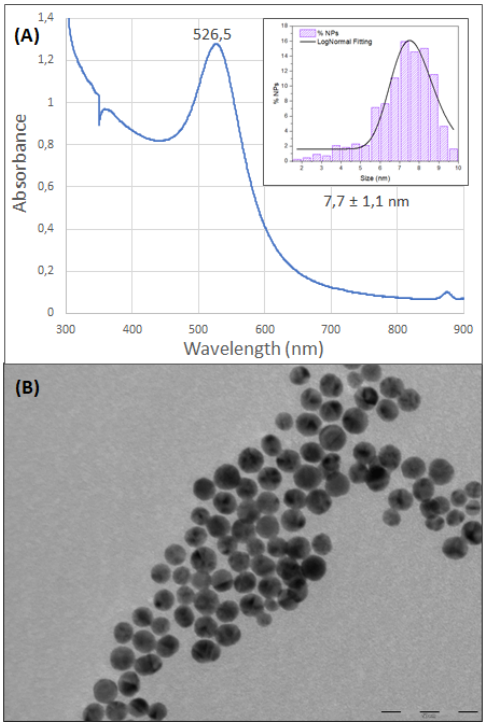

Figure 1: Characterization results of AuNPs: (A) UV-visible spectrum with peak calculation and size distribution histogram; (B) TEM image with 200kX of magnification.

The UV-visible spectra obtained (as represented on figure 1A) demonstrate high colloidal stability since at high wavelengths, the absorbance is practically zero. Also, there was a peak obtained at 526,5 nm, which is accordingly to the expected since the SPR of spherical AuNPs creates an absorption peak in the visible region (from 520 nm to 580 nm).[17]

Finally, the TEM images obtained (figure 1B) show high monodispersity and a mean size of about 7,7 nm.

Gold Concentration

In order to use the AuNPs synthesized as seeds to grow a AuFe-based shell, it is required to know its gold concentration as a parameter to further calculate the amount of reagents used on the Au-AuFe core-shell nanoparticles synthesis protocol described on 2.1. Thus, it is possible to perform ICP-MS, which is a widely used technique to determine metal elements, with the intention of determining the gold concentration existing on the AuNPs synthesized. Nonetheless, this technique is highly time-consuming both for the preparation of the sample as well as for the waiting time of the results (a total of, minimum, 2 weeks). And, along with the fact that it leads to the deterioration of the sample, other alternatives were pursued. In this manner, the possibility of calculating the gold concentration of AuNPs from UV-visible spectra was explored. From the Lambert Beer's law[18] represented by equation (1), in which A is the absorbance, ε the molar absorption coefficient ($M^{-1}cm^{-1}$), c the concentration in molar (M) and l the optical path in cm, it is viable to consider a linear correlation between the absorbance obtained with UV-visible spectroscopy and the concentration of gold in the AuNPs. Particularly, in the case of gold, there's the advantage that its molar absorption coefficient at 400 nm has been precisely estimated and it's constant (2400 $M^{-1}cm^{-1}$) regardless of the shape and size of the NPs.[19]

$$A = \varepsilon c l \tag{1}$$

Hence, using equation (1) knowing that the optical path (i.e. cell width) is 1 cm, the AuNPs absorbance at 400nm and the ε_{400} of 2400 $M^{-1}cm^{-1}$, the gold concentration can be easily obtained. Furthermore, in order to obtain a more accurate value of concentration some dilutions were made in each synthesis and the final Au concentration was estimated as the average of concentrations of the different dilutions.

Stated this, it is possible to calculate the gold concentration from UV-visible spectrum as it is an accurate method, and it was performed on every following AuNPs synthesis as it is a faster, easier and cheaper method comparing to ICP-MS.

3.2. Au-AuFe Core-Shell NPs: Synthesis and Characterization

The protocol described on Section 2.2 for the hybrid NPs was tested in different synthesis conditions, namely the molar ratio of AuNPs seeds versus the gold and iron precursors, $Au(COOCH_3)_3$ and $Fe(CO)_5$, respectively, and the usage of two distinct solvents, octadecene and dioctyl ether.

3.2.1 Synthesis with $Au(COOCH_3)_3$

Primarily, the protocol was tested with a molar ratio of AuNPs seeds in relation to $Au(COOCH_3)_3$ and $Fe(CO)_5$ of 1:1:1, both using octadecene and dioctyl ether, leading to samples SS21 and SS22, respectively. Subsequently, the amount of precursors used was increased to the double of AuNPs, translating into a ratio of 1:2:2, and it was also tested using octadecene and dioctyl ether as solvents, leading to samples SS30 and SS33, respectively.

On figure 2, the synthesis parameters and respective TEM images and UV-vis spectra of both the initial AuNPs and final NPs obtained are represented.

Characterization:

SS21 TEM images of SS21 (figure 2) present a few dimers and show three different sizes of nanoparticles.

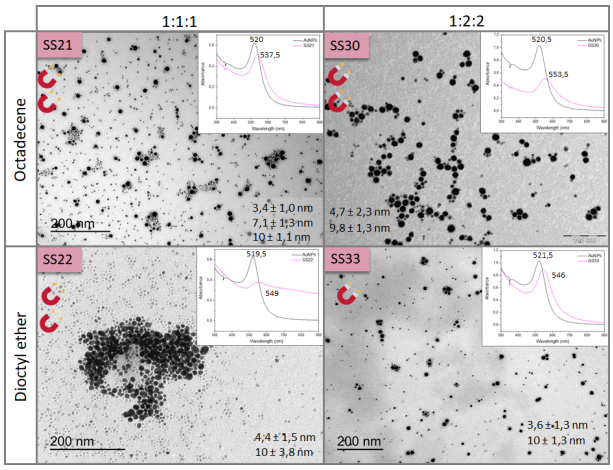

Figure 2: TEM images and UV-visible spectra of both AuNPs seeds and final NPs for the synthesis with gold precursor.

Additionally, comparing to the size of the initial AuNPs, there is the formation of lower-sized NPs, indicating that new NPs have been formed, beyond the possible formation of Au-AuFe core-shell nanoparticles. In the UV-visible spectra of sample SS21 along with the respective AuNPs seeds (figure 2), it is noticeable that at high wavelengths the absorbance in both spectra is null, suggesting good monodispersity and probably the absence of aggregates. Furthermore, there is a shift of 17,5 nm from the LSPR peak of the initial AuNPs, implying its surface modification.

Since TEM images demonstrate the existence of three different sizes of NPs, it is important to analyze the composition of each group size of nanoparticles, in order to have a better understanding of its composition.

This way, HRTEM was performed and the results are described on figure 3A, along with an analysis of its crystalline plans by Digital Microsoft.

The crystalline plan analysis revealed only the presence of Au in the NPs formed, however it is visible in the HRTEM images the presence of lighter domains that suggest the existence of Fe_3O_4 in the sample, which is concordant to the fact that the sample is highly magnetic (as demonstrated on figure 2).

Thus, an EDX analysis was carried out to find out the percentage of both Fe and Au presented on the sample. The EDX analysis (figure 3B) was achieved in regions where a group of NPs is visible and in regions where only a couple of NPs are visible, and the results demonstrate an Fe percentage of about 9% and 20%, respectively. Nevertheless, the percentage obtained when a group of NPs are analyzed is a more realistic approach than the one obtained when only a few NPs are considered, since it is a global measurement and the risk of contamination is lower.

Some small grayer domains were observed, although an analysis by HRTEM was not possible. Hence the Fe percentage determined by EDX could be due to the formation of Fe_3O_4 rather than metallic Fe.

Therefore, an analysis of XPS was taken place to determine the oxidation state of the existing Fe, and the results for the high resolution XPS spectrum of Fe 2p of sample SS21 is showed on figure 3C.

Analysing figure 3C, there are no visible peaks on the XPS spectrum of Fe 2p of sample SS21, which is not in agreement neither to the EDX analysis (figure 3B), that shows a considerable Fe percentage, nor to the fact that the sample has a high response to the magnet. In order to make sure that the XPS data obtained was in fact correspondent to the sample studied, this measurement was repeated and the results obtained for the general surface's measurements indicate, once again, the absence of Fe, since no peak is visible around 700 eV of binding energy.

Subsequently, XRD analysis was also performed, aiming to examine crystalline phases present within the sample.

The XRD spectrum obtained for sample SS21 together with the reported crystallographic plans list for the Au and Fe_3O_4 phases (0011140 and 00-019-0629, respectively), along with the respective peak analysis is represented on figure 3D. The peaks observed seem to correspond only to Au, thus suggesting the absence of any Fe-based phase and thus confirming the results obtained by XPS (figure 3C).

The absence of Fe inferred by both XPS and XRD analysis is not concordant to the high magnetic susceptibility presented by this sample (as referenced on figure 2). A repetition of the synthesis of this sample should be performed, in order to discard any sample confusion during the sample's labeling process.

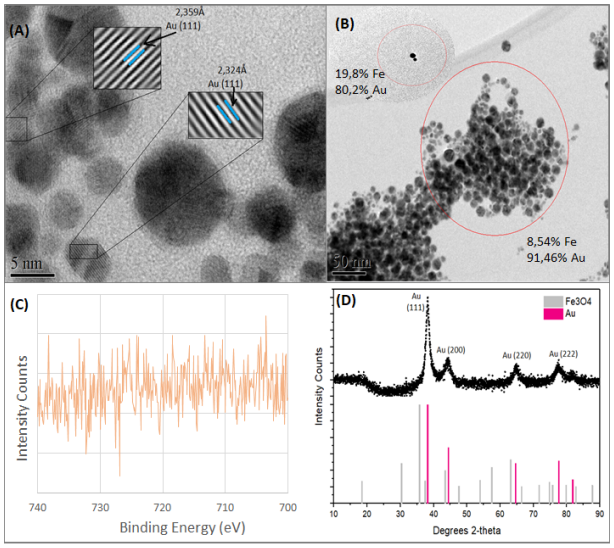

Figure 3: Characterization results of sample SS21: (A) HRTEM image and crystalline plan analysis; (B) EDX analysis results; (C) High resultion XPS spectrum of Fe 2p; (D) XRD results and peak analysis.

SS22 Concerning the synthesis of SS22, both TEM images and UV-visible spectrum (figure 2) indicate

the presence of aggregates. The UV-visible spectrum presents a shift of 28,5 nm from the initial AuNPs seeds. On TEM images, it is visible that there are two sizes of NPs, being the lower-sized nanoparticles smaller than the original AuNPs seeds used, suggesting the formation of new smaller nanoparticles.

Due to the great amount of aggregates observed indicating low colloidal stability, no further characterization techniques were carried out on this sample throughout this work.

SS30 As demonstrated by figure 2, the UV-visible spectrum of SS30 compared to the spectrum of the respective AuNPs seeds shows a shift of 58,5 nm on the LSPR peak of the initial AuNPs. TEM images show the presence of dimers along with two different sizes of nanoparticles, suggesting the possibility of the presence of either a Au-AuFe core-shell NPs or an overgrowth onto the AuNPs initial seeds, but also of newly formed Au or AuFe hybrid NPs.

In order to acquire more detailed information about the existence of the AuFe alloy on either the smaller and larger NPs observed, HRTEM images were obtained, which are exhibited on figure 4A, along with the respective crystalline plan analysis.

The crystalline plan analysis of HRTEM images illustrate the existence of AuNPs with either a shell or dimers of Fe_3O_4. In addition, EDX analysis was carried out on the HRTEM images obtained (figure 4B), and the results demonstrate an iron percentage of about 10%, that is concordant when analysing either a major group of NPs or just a few NPs. Hence, this quantity of Fe can probably be attributed to the Fe_3O_4 shell observed on HRTEM, although an AuFe alloy can exist in the interface between the Fe_3O_4 shell and the AuNPs surface.

This way, to evaluate the degree of oxidation of the existent iron, an XPS analysis was taken place, and the high resolution XPS spectrum of Fe 2p of sample SS30 is represented on figure 6A.

Contrarily to the XPS results obtained for the previous sample (SS21), on sample SS30 two peaks are observable on the Fe spectrum: one with 711,7 eV and the other with 726,7 eV of binding energy, being the first one the most accentuated peak. Consulting the bibliography on the binding energies for each material,[20] the first peak observed fits into the published information for the Fe $2p_{3/2}$ and the second one represents the $2p_{1/2}$ for the ion Fe^{3+}, which are symmetric peaks and thus represent the existence of Fe_3O_4 on this sample.

Although the high width observed on the first peak can be translated into a mixture of more than one oxidized state, in which metallic iron can be included, it is very difficult to claim the existence of an AuFe alloy given this data.

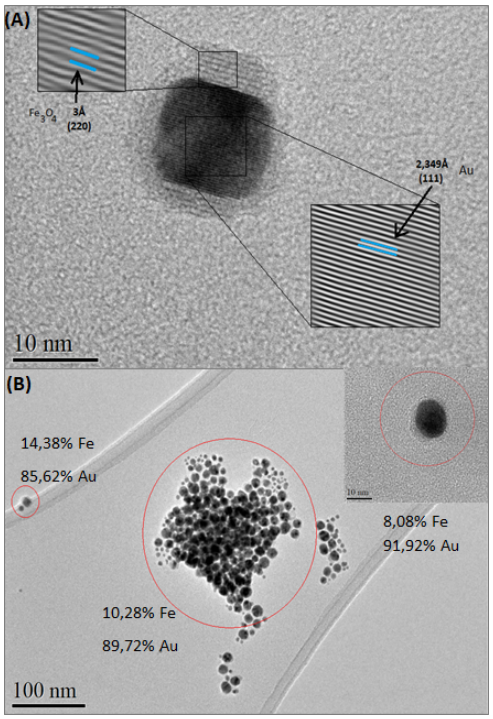

Figure 4: Characterization results of sample SS30 (A) HRTEM image and crystalline plan analysis; (B) EDX analysis.

SS33 Likewise for the samples mentioned above, UV-visible spectra and TEM images of both sample SS33 and respective AuNPs seeds (figure 2) demonstrate interesting results on colloidal stability, along with the formation of two different sizes of NPs.

Moreover, its UV-visible spectrum (figure 2) exhibits a shift of 24,5 nm from the original AuNPs, demonstrating a conformational change in relation to the initial AuNPs, and according to its TEM images, in which two different NPs sizes are visible, one of them has a smaller size comparing to the original AuNPs, thus again inferring the formation of newly formed NPs.

This way, this sample was also submitted to HRTEM to have a better understanding of its composition, as represented on figure 5A, and the crystalline plans found were analysed with Digital Microsoft software.

The crystalline plans analysis suggested only the presence of Au, which can be a positive data towards our objective, since the absence of Fe_3O_4 domains can be a good indicative for the presence of an AuFe alloy, considering that upon the formation of an AuFe alloy, the iron contained within is protected from oxidation.

Since only the Au crystalline plans were detected, an EDX analysis was also performed in order to determine the Fe percentage contained in the characterized sample.

The EDX results expressed on figure 5B, consistently reveal an Fe percentage of about 10% to 90% of Au, which is concordant to the previous sample analyzed (SS30), since the only protocol difference between both samples is the solvent used (figure 2).

Contrarily to what was observed on HRTEM images

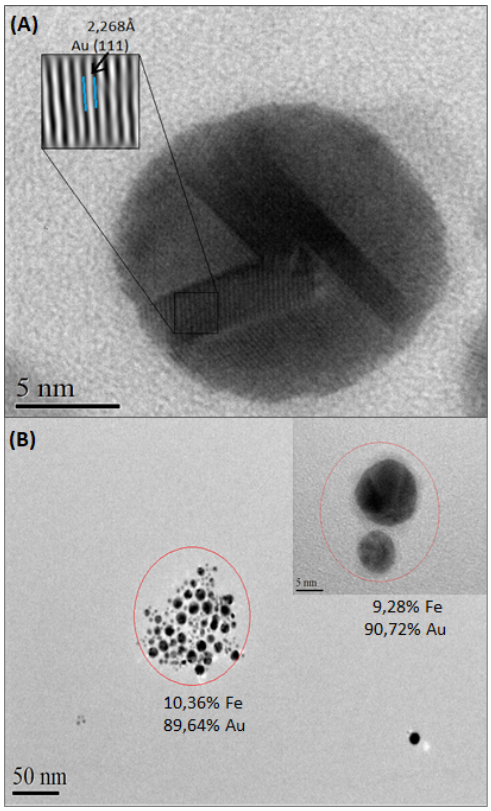

Figure 5: Characterization results of sample SS33 (A) HRTEM image and crystalline plan analysis; (B) EDX analysis.

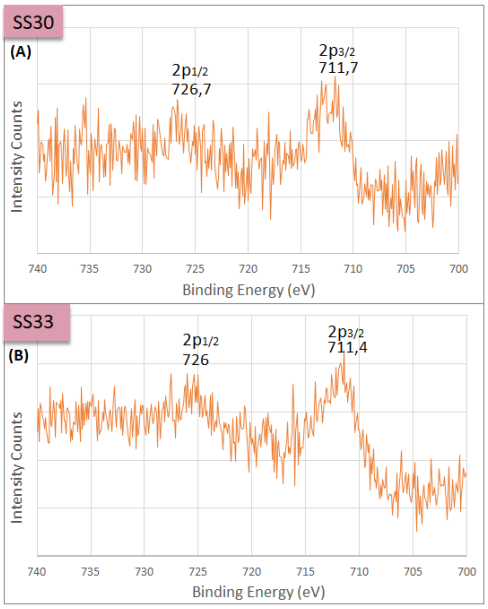

Figure 6: High resolution XPS spectra for the energy ranges corresponding to Fe 2p of (A) sample SS30 and (B) sample SS33.

for sample SS30, on sample SS33 no Fe_3O_4 domains are detected, and along with an Fe percentage of 10% detected with EDX, it is important to determine whether the sample contained metallic Fe or Fe_3O_4, hence the sample was submitted to an XPS analysis.

The XPS results for the high resolution Fe spectrum observable on figure 6B reveal the existence of two peaks, likewise to the previous sample, one accentuated peak with a value of 711,4 eV and another one with 726 eV of binding energy, which are very similar values to the ones obtained on sample SS30, meaning that Fe_3O_4 seems to be predominant on this sample, being the first peak registered correspondent to Fe $2p_{3/2}$ and the second one Fe $2p_{1/2}$.

Again, the Fe_3O_4 peak observed, as stated above, can present a wider form due to the existence of a mixture of different chemical states of iron, which does not exclude completely the possibility of having an AuFe alloy.

Exceptionally for this sample, the supernatant obtained upon washing had a darker color that the ones obtained for previous samples, which is translated into the existence of possibly smaller NPs that were unable to precipitate. This way, it was decided to characterize this supernatant obtained as well, in order to determine its composition.

SS33-Supernatant

The supernatant separated from the precipitate of sample SS33 was firstly characterized with UV-visible spectroscopy and TEM, comparing its results to the ones obtained for the initial AuNPs used, as demonstrated by figure 7.

TEM images (figure 7B) demonstrate that the NPs contained on the supernatant have a mean size of 3,3 nm, which is smaller than the size of the AuNPs used as seeds on this synthesis, meaning that these are NPs formed afterwards and have no relation to the AuNPs added into the reaction mixture.

This way, HRTEM was also performed in order to realize if these NPs contain Fe and/or Au. The HRTEM images and correspondent crystalline plan analysis is represented on figure 8A.

The analysis of the crystalline plans reveals the presence of peaks corresponding to only Au. Taking into account that no iron oxide NPs were detected on these HRTEM images, along with the fact that the supernatant solution hasn't showed magnetism (figure 2, which can also be due to its low concentration), most probably implies that these NPs are either only composed by Au or the alloy desired has been formed. Thus, an EDX analysis was also performed to make sure that the NPs formed are only composed by gold.

Interestingly, the EDX results displayed on figure 8B showed an amount of 20% of Fe in relation to 80% of Au, which is a considerable quantity of Fe and can be related to the existence of an AuFe alloy on these small NPs newly formed. Consequently, an XPS global analysis was also performed, which suggested the presence of Fe, since a peak is visible around 700 eV of binding energy. Even though this peak is less visible than the ones observed on samples SS30 and SS33, it is possible to assume the presence of either metallic Fe or Fe_3O_4 in this sample.

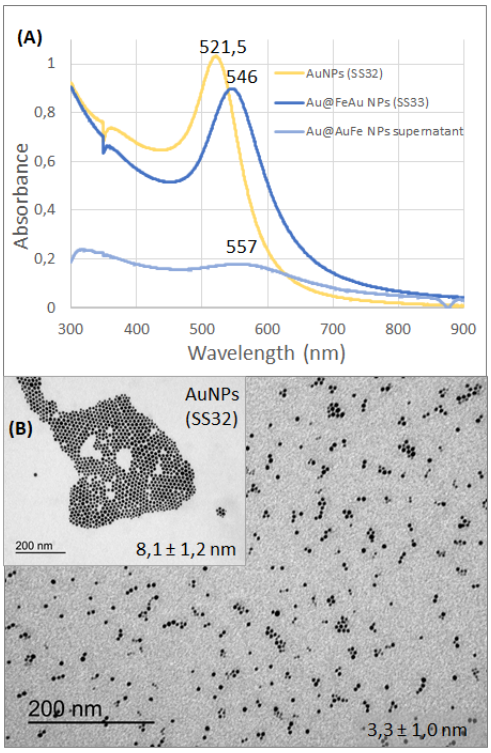

Figure 7: Characterization results of supernatant of sample SS33: (A) UV-visible spectrum with peak calculation of SS33, supernatant of SS33 and respective AuNPs; (B) TEM images of supernatant of SS33 and respective AuNPs.

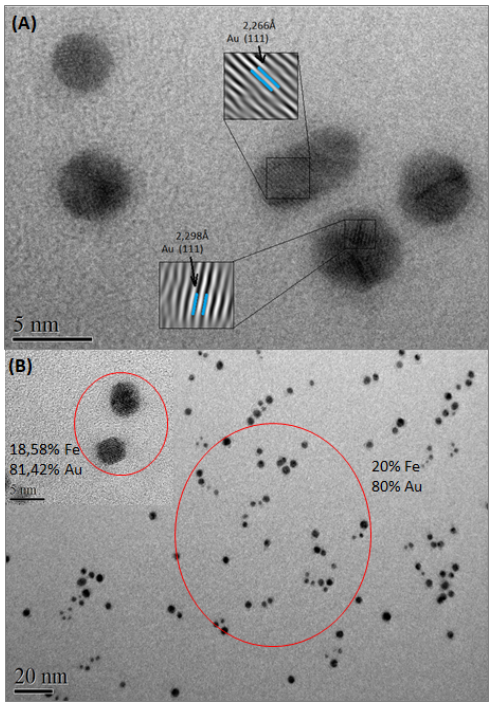

Figure 8: Characterization results of supernatant of sample SS33 (A) HRTEM image and crystalline plan analysis; (B) EDX analysis.

Overall, the shapes obtained were nearly spherical, except for the sample SS22, in which the NPs formed suffered coalescence, thus forming irregular shaped particles and aggregates. Regarding the solvent, the use of octadecene seems to favor the formation of dimers and shells, although the usage of dioctyl ether seems to lead to rounder nanoparticles. The choice of doubling the amount of $Au(COOCH_3)_3$ and $Fe(CO)_5$ in relation to AuNPs seeds derived from the idea that if there is excess of precursors in relation to AuNPs, it would facilitate the formation of an hybrid AuFe shell, which from the TEM images obtained it is not possible to confirm if it worked, since the images were taken by low resolution TEM and there is not a substantial growth observed from the samples SS21 and SS30, where the molar ratio of AuNPs:Au:Fe was 1:1:1, and the samples SS22 and SS33 in which the same molar ratio was 1:2:2.

As we have observed for all these samples the formation of new Au or AuFe NPs, we have adapted the synthesis aiming at avoiding the formation of these new NPs by not adding the $Au(COOCH_3)_3$ precursor to the reaction system.

3.2.2 Synthesis without $Au(COOCH_3)_3$

All the synthesis performed without using the gold precursor, $Au(COOCH_3)_3$, were performed using a molar ratio of AuNPs seeds to $Fe(CO)_5$ (AuNPs:Fe) of 1:1.

At first, the protocol of was tested at higher temperatures: after reacting for one hour at 250°C, the temperature was increased until 290°C (closer to the solvent's boiling point as possible) for half an hour, using once again distinct solvents, octadecene and dioctyl ether, hence leading to samples SS24 and SS25, respectively. Afterwards, the protocol was tested at lower temperatures, and instead of having 250°C for one hour, the temperature was decreased to 180°C for two hours. Once again, octadecene and dioctyl ether were used to perform the same protocol, resulting into samples SS27 and SS28, respectively.

The UV-visible spectra and TEM images resulted on these synthesis, along with the synthesis parameters used, are described on figure 9.

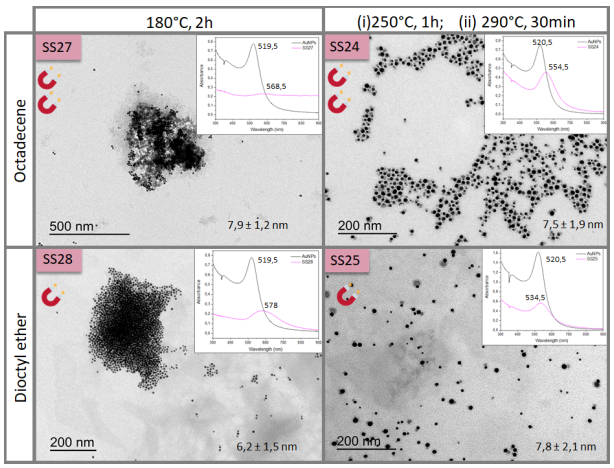

Figure 9: TEM images and UV-visible spectra of both AuNPs seeds and final NPs for the synthesis excluding gold precursor, along with the respective synthesis parameters.

Comparing to the synthesis including gold precursor (figure 2), it is visible that there is only one size of nanoparticles when excluding the $Au(COOCH_3)_3$, suggesting that the formation of smaller AuNPs from the precursor was avoided, as intended. However, when using the protocol at lower temperatures for longer (samples SS27 and SS28, 180°C for 2h), a great amount of aggregates are observed, meaning that the samples are not colloidally stable. Thus, more interesting samples are obtained when using higher temperatures (samples SS24 and SS25, 250°C for one hour and 290°C for half an hour), although there is also the formation of what appears to be Fe_3O_4 domains.

Comparing the solvent used, the protocol was tested using both octadecene and dioctyl ether, in which it has been reported by E. Fantechi et al.[21] that the morphology can be tuned from dimer to flower-like by increasing solvent polarity. In this work, when using octadecene, flower-like NPs are obtained, contrariwise to the dimers obtained when using dioctyl ether, which is accordingly to the expected since the different polarities of the solvents lead to NPs with different morphologies.

Additionally, samples SS27 and SS28 present magnetism, as described on figure 9 (less than samples SS24 and SS25 (figure 2)), therefore there is the presence of either metallic Fe or Fe_3O_4 into the NPs formed, since Au does not present magnetism.

Regarding the UV-visible spectra obtained (figure 9), a peak shift between the initial AuNPs and the final NPs was registered on all the samples mentioned, being 34 nm for sample SS24, 14 nm for sample SS25, 49 nm for SS27 and 58,5 nm for SS28, which is accordant to the expected since a higher amount of aggregates leads to a greater peak shift.

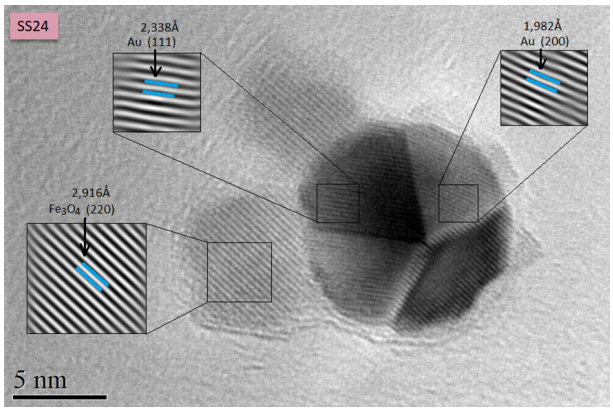

Figure 10: HRTEM image of sample SS24 and respective crystalline plan analysis.

Overall, UV-visible spectra obtained for all the samples mentioned above present wider peaks than the ones observed for the respective AuNPs seeds, meaning that there are different sizes of NPs in the same sample, and can be indicative to an AuFe alloy. However, in the samples where the $Au(COOCH_3)_3$ was excluded, the formation of either aggregates or Fe_3O_4 domains was observed. In fact, since in the low resolution TEM images it is not reliable to claim that the grayer domains are in fact Fe_3O_4, the sample SS24 (that present the biggest grayer domains) was submitted to HRTEM, and the crystalline plans were then analysed with Digital Microsoft software. It was confirmed the existence of AuNPs with Fe_3O_4 domains on its surface, as demonstrated on figure 10.

On figures 2 and 9, the magnets beside each sample represent the experiment that was preformed after each synthesis in which a powerful magnet was used to test whether the sample presents magnetic response or not. In the samples where there are two magnets instead of only one it means that the sample reacts greatly to the magnet, resulting in a qualitative analysis of the magnitude of its magnetic susceptibility.

Concluding, most probably when excluding the $Au(COOCH_3)_3$, the AuFe alloy is not formed. On the other hand, when $Au(COOCH_3)_3$ was used, new NPs were formed. In any of the two protocols it cannot be completely proven the presence of AuFe alloy either as a shell of the preformed AuNPs or in the form of the newly NPs arisen.

3.3. UV-Visible Spectroscopy

Since the NPs studied in this work contained gold, the evaluation of its optical properties was crucial, hence UV-visible spectroscopy was a widely used technique throughout all the experiment procedures. Furthermore, a Cary 100 UV-visible spectrophotometer was used in this work and it's designated as a double beam optical system.[22]

The UV-visible spectra compare the AuNPs seeds with the Au-AuFe core-shell NPs, however the gold nanoseeds solvent is hexane while toluene is the solvent of the core-shell NPs. Since the base line used to obtain each spectrum was achieved by using the solvent of each sample, the spectra that compare both NPs can present a shift related to the different polarities of the solvents used, that present different dielectric constants.

In order to evaluate the magnitude of this shift, UV-visible spectra were obtained with the same sample of AuNPs, using toluene and hexane as base lines, resulted on a peak shift of about 3,5-4 nm, which can be translated into the contribution of polarities differences between each solvent.

This analysis show that the peak shift observed on UV-visible spectra is mainly due to reasons other than the different solvents used, such as different sized nanoparticles and/or with different compositions. Hence, the observations concluded on sections above are considered accurate.

4. Conclusions and Future Work

The main goal of this work was to synthesize multifunctional Au-AuFe core-shell nanoparticles to be used on multiple biomedical applications. Although the synthesis of the desired spherical nanoparticles was not

achieved, it was possible to obtain nanoparticles with a mean size of 3,3 nm and containing about 20% of iron and 80% of gold, which is the maximum amount of iron we would be able to obtain on an AuFe alloy, since it is accordant to the obtained by the original protocol.

Furthermore, it was possible to conclude that through a colloidal synthesis it is very difficult to obtain the AuFe alloy as a shell. Futurely, since higher temperatures demonstrated to lead to better results, it would be interesting to use a non-colloidal synthesis in which more energy (i.e. higher temperature) is provided in order to promote the binding between gold and iron.

Concluding, even though there are some synthesis strategies of Au-Fe based hybrids, most studies based on these hybrids are still in a proof-of-concept stage, highlighting a need to establish detailed preclinical studies.

5. Acknowledgements

The work described herein was performed at the University of Barcelona, into both the Chemistry Department and the Physics Department, during the period from March to October of 2021, under the supervision of professors Xavier Batlle Gelabert and Marta Estrader Bofarull, within the frame of the Erasmus$^+$ Work Placements programs. This work was also co-supervised at Instituto Superior Técnico by professor Maria Clara Gonçalves.

A special thank to Víctor Fernàndez-Altable, Mariona Escoda I Torroella and Amilcar Ramon Labarta Rodriguez for all the guidance and valuable discussions.

References

[1] Anca Onaciu, Cornelia Braicu, Alina-Andreea Zimta, Alin Moldovan, Rares Stiufiuc, Mihail Buse, Cristina Ciocan, Smaranda Buduru, and Ioana Berindan-Neagoe. Gold nanorods: From anisotropy to opportunity. an evolution update. *Nanomedicine*, 14(9):1203–1226, 2019.

[2] Jose E Ortiz-Castillo, Roberto C Gallo-Villanueva, Marc J Madou, and Victor H Perez-Gonzalez. Anisotropic gold nanoparticles: A survey of recent synthetic methodologies. *Coordination Chemistry Reviews*, 425:213489, 2020.

[3] Asahi Tomitaka, Hamed Arami, Arash Ahmadivand, Nezih Pala, Anthony J McGoron, Yasushi Takemura, Marcelo Febo, and Madhavan Nair. Magneto-plasmonic nanostars for image-guided and nir-triggered drug delivery. *Scientific reports*, 10(1):1–10, 2020.

[4] Farzaneh Fathi, Mohammad-Reza Rashidi, and Yadollah Omidi. Ultra-sensitive detection by metal nanoparticles-mediated enhanced spr biosensors. *Talanta*, 192:118–127, 2019.

[5] Ana Espinosa, Javier Reguera, Alberto Curcio, Álvaro Muñoz-Noval, Christian Kuttner, Aurore Van de Walle, Luis M Liz-Marzán, and Claire Wilhelm. Janus magnetic-plasmonic nanoparticles for magnetically guided and thermally activated cancer therapy. *Small*, 16(11), 2020.

[6] Sabine Szunerits, Tamazouzt Nait Saada, Dalila Meziane, and Rabah Boukherroub. Magneto-optical nanostructures for viral sensing. *Nanomaterials*, 10(7):1271, 2020.

[7] Elyahb Allie Kwizera, Elise Chaffin, Yongmei Wang, and Xiaohua Huang. Synthesis and properties of magnetic-optical core–shell nanoparticles. *RSC advances*, 7(28):17137–17153, 2017.

[8] Maria V Efremova, Marina Spasova, Markus Heidelmann, Ivan S Grebennikov, Zi-An Li, Anastasiia S Garanina, Iana O Tcareva, Alexander G Savchenko, Michael Farle, Natalia L Klyachko, et al. Room temperature synthesized solid solution aufe nanoparticles and their transformation into au/fe janus nanocrystals. *Nanoscale*, 2021.

[9] Mariam Abdulaziz M Tarkistani, Varsha Komalla, and Veysel Kayser. Recent advances in the use of iron–gold hybrid nanoparticles for biomedical applications. *Nanomaterials*, 11(5):1227, 2021.

[10] Adawiya J Haider, Maha A Al-Kinani, and Sharafaldin Al-Musawi. Preparation and characterization of gold coated super paramagnetic iron nanoparticle using pulsed laser ablation in liquid method. In *Key Engineering Materials*, volume 886, pages 77–85. Trans Tech Publ, 2021.

[11] I-C Chiang and D-H Chen. Synthesis of monodisperse feau nanoparticles with tunable magnetic and optical properties. *Advanced Functional Materials*, 17(8):1311–1316, 2007.

[12] Chengmin Shen, Chao Hui, Tianzhong Yang, Congwen Xiao, Jifa Tian, Lihong Bao, Shutang Chen, Hao Ding, and Hongjun Gao. Monodisperse noble-metal nanoparticles and their surface enhanced raman scattering properties. *Chemistry of Materials*, 20(22):6939–6944, 2008.

[13] Baojun Liu and Xia Hu. Hollow micro-and nanomaterials: Synthesis and applications. In *Advanced Nanomaterials for Pollutant Sensing and Environmental Catalysis*, pages 1–38. Elsevier, 2020.

[14] RT Downs, KL Bartelmehs, GV Gibbs, and MB Boisen. Interactive software for calculating and displaying x-ray or neutron powder diffractometer patterns of crystalline materials. *American Mineralogist*, 78(9-10):1104–1107, 1993.

[15] Howard Eugene Swanson. *Standard X-ray diffraction powder patterns*, volume 25. US Department of Commerce, National Bureau of Standards, 1971.

[16] Balaprasad Ankamwar. Size and shape effect on biomedical applications of nanomaterials. *Biomedical Engineering-Technical Applications in Medicine*, pages 93–114, 2012.

[17] Wolfgang Haiss, Nguyen TK Thanh, Jenny Aveyard, and David G Fernig. Determination of size and concentration of gold nanoparticles from uv- vis spectra. *Analytical chemistry*, 79(11):4215–4221, 2007.

[18] Dong-Kwan Kim, Yoon Jo Hwang, Cheolho Yoon, Hye-On Yoon, Ki Soo Chang, Gaehang Lee, Seungwoo Lee, and Gi-Ra Yi. Experimental approach to the fundamental limit of the extinction coefficients of ultra-smooth and highly spherical gold nanoparticles. *Physical Chemistry Chemical Physics*, 17(32):20786–20794, 2015.

[19] Leonardo Scarabelli, Ana Sánchez-Iglesias, Jorge Pérez-Juste, and Luis M Liz-Marzán. A "tips and tricks" practical guide to the synthesis of gold nanorods. *The Journal of Physical Chemistry Letters*, 6(21):4270–4279, 2015.

[20] Toru Yamashita and Peter Hayes. Analysis of xps spectra of fe2+ and fe3+ ions in oxide materials. *Applied surface science*, 254(8):2441–2449, 2008.

[21] Elvira Fantechi, Claudia Innocenti, Giovanni Bertoni, Claudio Sangregorio, and Francesco Pineider. Modulation of the magnetic properties of gold-spinel ferrite heterostructured nanocrystals. *Nano Research*, 13(3):785–794, 2020.

[22] Agilent. The basics of uv-vis spectrophotometry, October 2021. Accessed 13-October-2021.